2018 IEEE Intelligent Vehicles Symposium (IV)
Changshu, Suzhou, China, June 26-30, 2018

Research on Modeling of Distributed Compound Braking System and Braking Force Allocation Strategy*

Jun Yao, Guoying Chen, Changfu Zong, Yaohua Guo

***Abstract*—This paper proposes a novel braking force allocation strategy for electric vehicles with four in-wheel motors (IWM). Based on the principle of maximizing the regenerative braking torque of four motors, the motor and the hydraulic braking force of both front and rear axles have been allocated to four wheels respectively, and the fuzzy control method is adopted to control the vehicle's slip rate under the emergency braking. The paper first analyzes two common regenerative braking control methods of IWM: half-bridge modulation and full-bridge modulation, and compares the modulation effect of the two control methods. Then, the braking force allocation strategy is proposed, which can be divided into two parts: under normal braking and under emergency braking. Finally, the braking force allocation strategy is verified through the co-simulation platform of Carsim, Matlab/Simulink and AMEsim. The simulation results show that under normal braking, the proposed braking force allocation strategy can preferentially adopt the motor braking force according to the maximum motor braking force. When the total braking force provided by the motors cannot meet the vehicle's braking severity requirements, EHB system involves in braking to provide the remaining braking force. Under emergency braking, the slip rate can be well controlled by the fuzzy control method.**

I. INTRODUCTION

Due to the independent control of four wheels, electric vehicles with four IWMs have many advantages over conventional combustion engine-powered vehicles. The electric vehicle with four IWMs is driven by the distributed power. And through the control of the inverters, the regenerative brake can be realized. Because the power of the motor is limited and IWM cannot provide braking torque at low speed, the EHB system must be retained in the electric vehicle with four IWMs.

Many scholars have studied the strategy of the compound brake control. Gao Yimin et al proposed three different braking control strategies for braking with optimal feel, braking with optimal energy recovery and parallel braking (Gao et al., 1999; Gao et al.,2001). For the electric vehicle with four IWMs, Wang B et al proposed a novel predictive-based robust controller for tracking the desired wheel slip ratio to prevent wheel locking by combining the hydraulic and regenerative braking systems (Wang et al., 2014). Wei Xu et al proposed a method to allocate the regenerative braking force using a model predictive control method for an electric vehicle with four IWMs and to optimize the cost function from three aspects (Xu et al.,2016). LIAN Yu-Feng et al proposed a new braking force distribution strategy based on regenerative braking severity continuity for electric vehicles with four-wheel drive (LIAN et al.,2009). Jianze Yu et al proposed a hierarchical control structure, consisting of an upper-layer adaptive sliding mode control and a lower-layer optimization-based control allocation algorithm (Yu et al.,2009).

This paper mainly studies the distributed compound braking system of the electric vehicle with four IWMs. For the distributed compound braking system, this paper proposes a novel braking force allocation strategy based on the principle of maximum motor braking force and verifies it by simulation.

II. REGENERATIVE BRAKING CONTROL MODEL OF IWM

The IWM adopted in the electric vehicles with four IWMs is permanent-magnet brushless DC motor (BLDC). Based on the assumption that the three-phase circuit of BLDC is symmetrical and the system parameters are constant, the voltage equation can be described as (1).

$$\begin{bmatrix} U_a \\ U_b \\ U_c \end{bmatrix} = \begin{bmatrix} R & 0 & 0 \\ 0 & R & 0 \\ 0 & 0 & R \end{bmatrix} \begin{bmatrix} I_a \\ I_b \\ I_c \end{bmatrix} + \begin{bmatrix} L-M & 0 & 0 \\ 0 & L-M & 0 \\ 0 & 0 & L-M \end{bmatrix} \frac{d}{dt} \begin{bmatrix} I_a \\ I_b \\ I_c \end{bmatrix} + \begin{bmatrix} E_a \\ E_b \\ E_c \end{bmatrix} \quad (1)$$

where U_a, U_b, U_c are the terminal voltages of the stator windings, R is the equivalent resistance value of the stator windings, and I_a, I_b and I_c are the current values through the stator windings, L is the inductance of the stator windings, M is the mutual inductance of the two stator windings, E_a, E_b and E_c are the induced electromotive force of the three-phase stator windings (Pillay et al., 1987).

The equivalent circuit based on the above model is shown in Figure 1, where T_1, T_2, T_3, T_4, T_5, T_6 are the switch tubes, and D_1, D_2, D_3, D_4, D_5, D_6 are the diodes, and U_d is the terminal voltage of the battery. With the change of three Hall sensor signals H_1, H_2, H_3, six states of the motor can be obtained, respectively as 101, 100, 110, 010, 011, 001. The corresponding motor back electromotive force waveforms are shown in Figure 2.

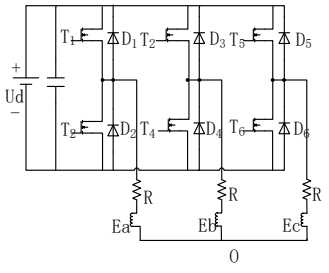

Figure 1. Equivalent circuit of BLDC.

Regenerative braking control methods of BLDC through chopper control can be divided into half-bridge modulation

*Research supported by National Natural Science Foundation of China (Grant No. 51505178) and China Postdoctoral Science Foundation (Grant NO.2014M561289).

G. C. Author is with State Key Laboratory of Automotive Simulation and Control, Jilin University, China (corresponding author to provide phone:135-7887-6030; e-mail: cgy-011@163.com).

J. Y. Author, C. Z. Author are with State Key Laboratory of Automotive Simulation and Control, Jilin University, China (e-mail: 18326184369@139.com; e-mail: 378811297@qq.com).

Y. G. Author is with Zhengzhou Yutong Bus Co. Ltd, China (e-mail: guoyhb@yutong.com)

and full-bridge modulation. In the half-bridge modulation process, only the switch tubes of the upper arm or lower arm have a switch action, and the three switch tubes of the other side of the arm are always in the cut-off state. The battery does not output power to the motor. However, during the full-bridge modulation process, the six switch tubes of the bridge are all pulse-width modulated, and the switch tube on-off logic of the forward braking is consistent with that of the reverse driving, so the battery will output a reverse current to the motor and this braking control method has a greater braking severity.

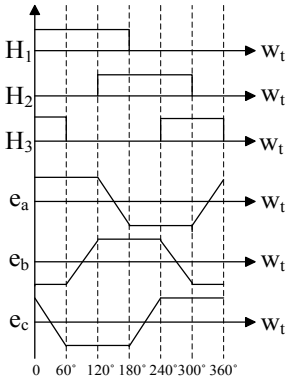

Figure 2. Motor back electromotive force waveform.

A. *Analysis of half-bridge modulation process*

It is assumed that the switch tubes(T_1,T_3,T_5) of the upper arm are always in the cut-off state, and the switch tubes(T_2,T_4,T_6) of the lower arm have the pulse-width modulation. The switch tube on-off logic of the half-bridge modulation is shown in TABLE I.

TABLE I. SWITCH TUBE ON-OFF LOGIC OF THE HALF-BRIDGE MODULATION

Hall State	101	100	110	010	011	001
Turn-on switch tube	T_2	T_2	T_4	T_4	T_6	T_6

The half-bridge modulation process of BLDC is analyzed with 101 Hall state as an example. From Figure 2, the motor's back electromotive force in 101 Hall state can be obtained.

$$E_\alpha=E,\ E_\beta=-E,\ -E<E_\chi<E.$$

where E is the maximum value of the back electromotive force. In 101 Hall state, only the switch tube T_2 is pulse-width modulated, and the modulation process can be divided into the following three cases.

***Case 1*: T_2** is on and E_c >0, and the system forms a freewheeling circuit, as shown in Figure 3.

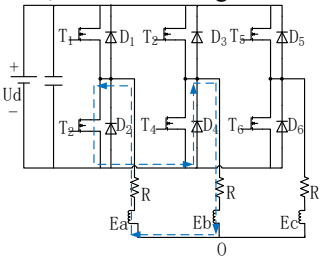

Figure 3. Equivalent circuit under *Case 1* during the half-bridge modulation.

Since the back electromotive force E_c> 0 and the motor midpoint electromotive force U_n = 0, C phase will be cut off. At this point, the system will form the circuit from A-phase to T_2, to D_4, to B-phase, and then back to the A-phase. So, the voltage equation can be described as

$$\begin{bmatrix}0\\0\\U_c\end{bmatrix}=\begin{bmatrix}R&0&0\\0&R&0\\0&0&R\end{bmatrix}\begin{bmatrix}I_a\\I_b\\I_c\end{bmatrix}+\begin{bmatrix}L\text{-}M&0&0\\0&L-M&0\\0&0&L-M\end{bmatrix}\frac{d}{dt}\begin{bmatrix}I_a\\I_b\\I_c\end{bmatrix}+\begin{bmatrix}E_a\\E_b\\E_c\end{bmatrix} \quad (2)$$

where $I_c = 0$, $I_a = -I_b$ and $E_a = -E_b = E$.

Case 2: T_2 is on and $E_c \le 0$, and the system forms a freewheeling circuit, as shown in Figure 4.

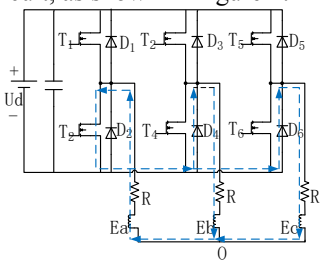

Figure 4. Equivalent circuit under *Case 2* during the half-bridge modulation.

When $E_c \le 0$ and $U_n = 0$, the diode D_6 is conducted. At this point, C-phase is turned on, and the system will form two loops. One is the circuit from A-phase to T_2, to D_4, to B-phase, and then back to the A-phase. The other is the circuit from A-phase to T_2, to D_6, to C-phase, and then back to the A-phase. The voltage equation can be described as (3):

$$\begin{bmatrix}0\\0\\0\end{bmatrix}=\begin{bmatrix}R&0&0\\0&R&0\\0&0&R\end{bmatrix}\begin{bmatrix}I_a\\I_b\\I_c\end{bmatrix}+\begin{bmatrix}L\text{-}M&0&0\\0&L-M&0\\0&0&L-M\end{bmatrix}\frac{d}{dt}\begin{bmatrix}I_a\\I_b\\I_c\end{bmatrix}+\begin{bmatrix}E_a\\E_b\\E_c\end{bmatrix} \quad (3)$$

where $I_c = 0$, $I_a = -I_b$ and $E_a = -E_b = E$.

During the freewheeling process, the equivalent circuit through inductance 2(L-M) and the current curve during the half-bridge modulation process are shown in Figure 5 and Figure 6, where T is the cycle time of modulation, t_0-t_1 is the freewheeling process, t_1-t_2 is the charging process, i_t is the current of the equivalent circuit at the end of the motor freewheeling process, and i_0 is the current of the equivalent circuit at the end of the charging process.

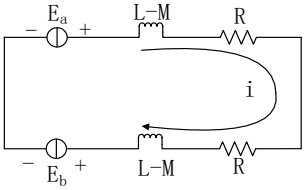

Figure 5. Freewheeling circuit during the half-bridge modulation.

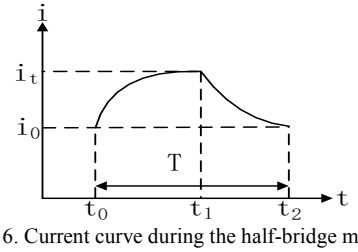

Figure 6. Current curve during the half-bridge modulation.

According to Kirchhoff's law, we can get:

$$U_L = 2(L-M)\frac{di}{dt}+2Ri=E_a-E_b \quad (4)$$

where U_L is the voltage drop across resistor $2R$ and inductor $2(L\text{-}M)$. Ignoring the voltage drop across the resistor $2R$, the energy accumulated on the inductance $2(L\text{-}M)$ during t_0 to t_1 is shown in (5).

$$W_{in}=\int_{t_0}^{t_1}(E_a-E_b)idt=\int_{t_0}^{t_1}2Eidt \tag{5}$$

Case 3: T_2 is off and the system forms a charging circuit, as shown in Figure 7.

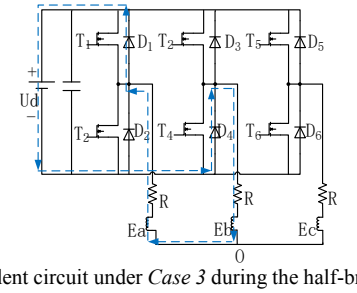

Figure 7. Equivalent circuit under *Case 3* during the half-bridge modulation.

When T_2 is off, due to the high self-induced electromotive force generated by the windings, the sum of the inductance induced electromotive force and the back electromotive force is greater than the battery voltage, making the motor windings charge the battery. At this point, the system will form the circuit from A-phase to D_1, to the battery, to D_4, to B-phase and then back to the A-phase. The voltage equation can be described as (6):

$$\begin{bmatrix}U_0\\0\\U_c\end{bmatrix}=\begin{bmatrix}R&0&0\\0&R&0\\0&0&R\end{bmatrix}\begin{bmatrix}I_a\\I_b\\I_c\end{bmatrix}+\begin{bmatrix}L\text{-}M&0&0\\0&L-M&0\\0&0&L-M\end{bmatrix}\frac{d}{dt}\begin{bmatrix}I_a\\I_b\\I_c\end{bmatrix}+\begin{bmatrix}E_a\\E_b\\E_c\end{bmatrix} \tag{6}$$

where U_0 is the charging voltage of the battery.

During the charging process, the equivalent circuit through inductance $2(L\text{-}M)$ is shown in Figure 8**.**

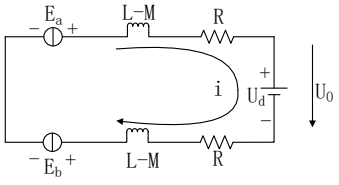

Figure 8. Charging circuit during the half-bridge modulation.

According to Kirchhoff's law, we can get:

$$U_L=2(L-M)\frac{di}{dt}+2Ri=U_0-(E_a-E_b) \tag{7}$$

Ignoring the voltage drop across the resistor $2R$, the energy released from the inductance 2 $(L\text{-}M)$ during t_1 to t_2 is

$$W_{out}=\int_{t_1}^{t_2}(U_0-(E_a-E_b))idt=\int_{t_1}^{t_2}(U_0-2E)idt \tag{8}$$

It is assumed that the energy released and accumulated by inductance $2(L\text{-}M)$ in one cycle is equal and the change of current in this process is ignored, then we can get

$$2Ei(t_1-t_0)=(U_0-2E)i(t_2-t_1) \tag{9}$$

And t_0, t_1, t_2 satisfy the relationship $\frac{t_1-t_0}{t_2-t_1}=\frac{\alpha}{1-\alpha}$, where α is the duty cycle. Then

$$U_0=\frac{2E}{1-\alpha} \tag{10}$$

When $U_0>U_d$, which also means $\alpha>\frac{U_d-2E}{U_d}$, the motor can charge the battery by the half-bridge modulation.

During the charging process, the current continuously reduces until $U_0<U_d$. At this time, the diode D_1 is cut off, and the charging circuit is interrupted. It can be seen that the battery cannot output power during the half-bridge modulation process.

B. Analysis of full-bridge modulation process

The switch tube on-off logic during the full-bridge modulation is shown in TABLE II.

TABLE III. SWITCH TUBE ON-OFF LOGIC OF THE FULL-BRIDGE MODULATION

Hall State	101	100	110	010	011	001
Turn-on switch tube	T_2T_3	T_2T_5	T_4T_5	T_1T_4	T_1T_6	T_3T_6

The full-bridge modulation process of BLDC is also analyzed with 101 Hall state as an example. The modulation process can be divided into the following two cases.

Case 1: T_2 and T_3 are on, and the system forms a freewheeling circuit, as shown in Figure 9.

When T_2 and T_3 are on, the system will form the circuit from A-phase to T_2, to the battery, to T_3, to B-phase and then back to the A-phase. At this point, the battery is charge for the inductance $2(L\text{-}M)$.

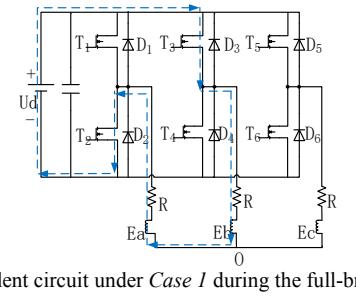

Figure 9. Equivalent circuit under *Case 1* during the full-bridge modulation.

When T_2 and T_3 are on, the system will form the circuit from A-phase to T_2, to the battery, to T_3, to B-phase and then back to the A-phase. At this point, the battery is charge for the inductance $2(L\text{-}M)$.

The voltage equation can be described as:

$$\begin{bmatrix}0\\U_0\\U_c\end{bmatrix}=\begin{bmatrix}R&0&0\\0&R&0\\0&0&R\end{bmatrix}\begin{bmatrix}I_a\\I_b\\I_c\end{bmatrix}+\begin{bmatrix}L\text{-}M&0&0\\0&L-M&0\\0&0&L-M\end{bmatrix}\frac{d}{dt}\begin{bmatrix}I_a\\I_b\\I_c\end{bmatrix}+\begin{bmatrix}E_a\\E_b\\E_c\end{bmatrix} \tag{11}$$

During the freewheeling process, the equivalent circuit through inductance $2(L\text{-}M)$ is shown in Figure 10.

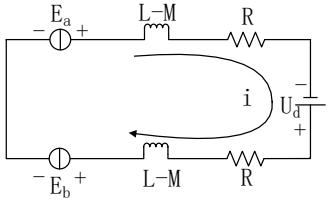

Figure 10. Freewheeling circuit during the full-bridge modulation.

According to Kirchhoff's law, we can get:

$$U_L = 2(L-M)\frac{di}{dt} + 2Ri = U_d + E_a - E_b \tag{12}$$

Ignoring the voltage drop across the resistor $2R$, the energy accumulated on the inductance $2(L\text{-}M)$ during t_0 to t_1 is

$$W_{in} = \int_{t_0}^{t_1}(U_d + E_a - E_b)idt = \int_{t_0}^{t_1}(U_d + 2E)idt \tag{13}$$

Case 2: T_2 and T_3 are off, and the system forms a charging circuit, as shown in Figure 11.

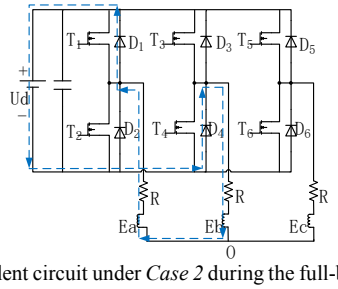

Figure 11. Equivalent circuit under *Case 2* during the full-bridge modulation.

When T_2 and T_3 are off, due to the high self-induced electromotive force generated by the windings, the motor windings is charge for the battery. At this point, the system will form the circuit from A-phase to D_1, to the battery, to D_4, to B-phase and then back to the A-phase. The voltage equation can be described as:

$$\begin{bmatrix} U_0 \\ 0 \\ U_c \end{bmatrix} = \begin{bmatrix} R & 0 & 0 \\ 0 & R & 0 \\ 0 & 0 & R \end{bmatrix}\begin{bmatrix} I_a \\ I_b \\ I_c \end{bmatrix} + \begin{bmatrix} L\text{-}M & 0 & 0 \\ 0 & L-M & 0 \\ 0 & 0 & L-M \end{bmatrix}\frac{d}{dt}\begin{bmatrix} I_a \\ I_b \\ I_c \end{bmatrix} + \begin{bmatrix} E_a \\ E_b \\ E_c \end{bmatrix} \tag{14}$$

During the charging process, the equivalent circuit through inductance $2(L\text{-}M)$ is shown in Figure 12.

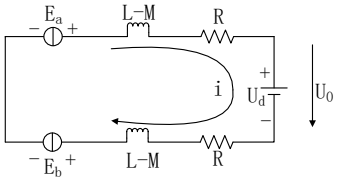

Figure 12. Charging circuit during the full-bridge modulation.

According to Kirchhoff's law, we can get:

$$U_L = 2(L-M)\frac{di}{dt} + 2Ri = U_0 - (E_a - E_b) \tag{15}$$

Similarly, the voltage drop across the resistor $2R$ is ignored, and the energy released on the inductor 2 $(L\text{-}M)$ during t_1-t_2 is

$$W_{out} = \int_{t_1}^{t_2}(U_0 - (E_a - E_b))idt = \int_{t_1}^{t_2}(U_0 - 2E)idt \tag{16}$$

It is also assumed that the energy released and accumulated by inductance $2(L\text{-}M)$ in one cycle is equal and the change of current in this process is ignored, then we can get

$$(U_d + 2E)i(t_1 - t_0) = (U_0 - 2E)i(t_2 - t_1) \tag{17}$$

And t_0, t_1, t_2 meet the relationship $\frac{t_1 - t_0}{t_2 - t_1} = \frac{\alpha}{1-\alpha}$, where α is the duty cycle. Then

$$U_0 = \frac{\alpha}{1-\alpha}U_d + \frac{2}{1-\alpha}E \tag{18}$$

When $U_0 > U_d$, which also means $\alpha > \frac{U_d - 2E}{2U_d}$, the motor can charge the battery by the full-bridge modulation.

During the charging process, the current continuously reduces until $U_0 < U_d$. At this time, the diode D_1 is cut off, and the charging circuit is interrupted. The charging process is as same as that of half-bridge modulation. The currents through the battery and the motor electromagnetic torque curves are shown in Figure 13 and Figure 14.

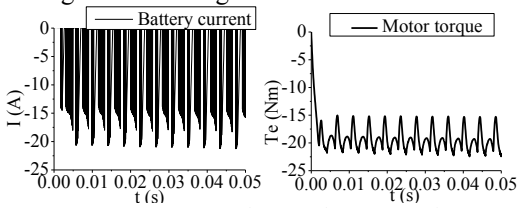

Figure 13. Battery current curve and motor electromagnetic torque curve of half-bridge modulation.

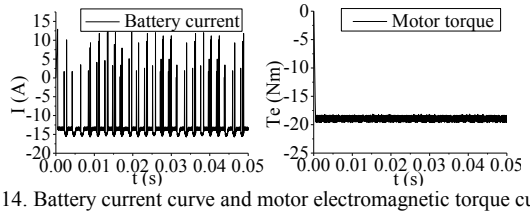

Figure 14. Battery current curve and motor electromagnetic torque curve of full-bridge modulation.

It can be found that during the half-bridge modulation process only the switch tubes of the upper arm or lower arm have the PWM action, and the cut-off phase can be conducted. Additionally, the torque ripple is large, and the maximum motor electromagnetic torque is small. The battery current is always negative, and the battery cannot output energy. During the full-bridge modulation process, the system is always two-phase conduction, and the battery will charge the inductance $2(L\text{-}M)$ during the freewheeling process. Torque ripple is small, and the maximum motor electromagnetic torque is large, with more obvious braking effect. In this paper, the full-bridge modulation is adopted to study the braking force allocation strategy.

III. Braking Force Allocation Strategy of Distributed Compound Braking System

Depending on whether the wheel locks, the braking process can be divided into normal braking and emergency braking. Under normal braking, the braking force allocation strategy is used to allocate the front and rear axle braking forces and the electro-hydraulic braking forces on each axis.

Under the emergency braking, in order to ensure the safety of the vehicle, slip rate of the vehicle will be the control target. At this point, the braking force is all provided by hydraulic braking force.

A. Braking Force Allocation Strategy under Normal Braking

The related parameter symbols are listed in TABLE III:

TABLE III. RELATED PARAMETERS TABLE

F_{μ}	The braking force required by the vehicle under the current braking severity
F_{I1}	The braking force required for the front axle under the ideal braking force curve distribution
F_{I2}	The braking force required for the rear axle under the ideal braking force curve distribution
F_{m1}	The maximum braking force that the front axle motor can provide at the current speed
F_{m2}	The maximum braking force that the rear axle motor can provide at the current speed
$F_{\mu1}$	The braking force assigned to the front axle under the control strategy
$F_{\mu2}$	The braking force assigned to the rear axle under the control strategy
$F_{\mu1m}$	The braking force provided by the front axle motor under the braking control strategy
$F_{\mu1f}$	The braking force provided by the front axle EHB system under the braking control strategy
$F_{\mu2m}$	The braking force provided by the rear axle motor under the braking control strategy
$F_{\mu2f}$	The braking force provided by the rear axle EHB system under the braking control strategy

In most papers on brake control strategy, the maximum braking torque of the motor is regarded as a fixed value. However, it can be seen from the characteristic curve of BLDC that the working point of the motor can be divided into constant torque zone and constant power zone. When the vehicle is running at high speed, the motor cannot provide maximum braking torque. In this paper, the maximum motor braking torque is obtained in real time according to the rotating speed of the motor. The front and rear axle braking force is allocated according to the maximum motor braking torque.

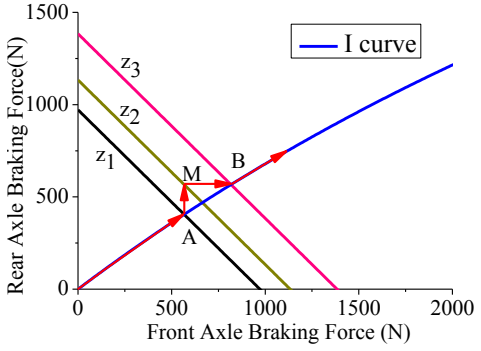

Figure 15. Curve of front and rear axle braking force allocation.

As shown in Figure 15, it can be found that when the front and rear axle braking forces are distributed according to the ideal braking force curve, the difference between them is large. Under some braking severities, the braking force required for the front axle has reached the maximum braking force that the motor can provide, but the motor braking force of the rear axle is not fully utilized. In order to make full use of the motor braking force, this paper proposes a novel braking control strategy based on the principle of maximizing motor braking force.

Front and rear axle braking force allocation

According to the braking severity, the front and rear axle braking force allocation can be divided into the following four stages:

(1) When the braking severity is less than z_1, $F_{\mu1} \le F_{m1}, F_{\mu2} \le F_{m2}$, the braking force of each axis can be provided by the motor braking force. Between O-A, the front and rear axle braking forces are allocated according to the ideal braking force distribution curve. Then, we can get

$$F_{\mu1} = F_{I1}, \quad F_{\mu2} = F_{I2} \tag{19}$$

When the point A is reached, the braking force required for the front axle is reached the maximum value that the front IWMs can provide. The threshold z_1 is calculated as follows:

From the ideal braking force distribution curve we can get:

$$F_{\mu1} = F_{m1} \tag{20}$$

$$F_{\mu2} = \frac{1}{2}\left[\frac{G}{h_g}\sqrt{b^2 + \frac{4h_g L}{G}F_{m1}} - \left(\frac{Gb}{h_g} + 2F_{m1}\right)\right] \tag{21}$$

Thus, z_1 is calculated by:

$$z_1 = \frac{F_{\mu1} + F_{\mu2}}{G} = \frac{2F_{m1} + \left[\frac{G}{h_g}\sqrt{b^2 + \frac{4h_g L}{G}F_{m1}} - \left(\frac{Gb}{h_g} + 2F_{m1}\right)\right]}{2G} \tag{22}$$

where G is the gravity of the vehicle, and h_g is the centroid height of the vehicle, and b is the distance from the center of mass to the rear axle, and L is the wheelbase of the vehicle.

(2) When the braking severity is between z_1 and z_2, $F_{\mu1} > F_{m1}, F_{\mu2} \le F_{m2}$ and $F_{\mu} \le F_{m1} + F_{m2}$. Although the front axle required braking force has exceeded the maximum braking force the front IWMs can provide, the total braking force provided by the four IWMs can still meet the vehicle's braking severity requirements. Between A-M, the front and rear axle braking force are not distributed according to the ideal braking force distribution curve, but the front axle braking force is equal to the maximum braking force that the front IWMs can provide and the remaining braking force is supplemented by the motors of the rear axle. EHB system does not participate in the braking process. Then, we can get

$$F_{\mu1} = F_{m1}, \quad F_{\mu2} = F_{\mu} - F_{m1} \tag{23}$$

Although the front and rear braking force distribution curve is located above the ideal braking distribution curve, the brake severity is small so that the dangerous condition like the front wheel first locks does not appear. When the M point is reached, the braking force required by the vehicle is exactly equal to the sum of the braking forces that the four IWMs can provide. The threshold z_2 is calculated as follows:

$$z_2 = \frac{F_{m1} + F_{m2}}{G} \tag{24}$$

(3) When the braking severity is between z_2 to z_3, the motor braking force has been unable to meet the needs of the braking severity. At this point, EHB system needs to participate in to supplement the vehicle required braking force. In order to ensure that there is no dangerous condition like the front wheel first locks, between M-B, the rear axle braking force is fixed to the maximum motor force that the rear axle motor can provide and the remaining braking force is provided by the front axle braking force. The front axle preferentially uses the motor braking force, and the remaining braking force is supplemented by the EHB system. Then, we can get

$$F_{\mu 1} = F_{\mu} - F_{m2}, \quad F_{\mu 2} = F_{m2} \tag{25}$$

When the braking severity reaches z_3, as shown in point B in the Figure 15, the braking force distribution curve intersects the ideal braking force distribution curve, and the braking severity z_3 is calculated as follows:

$$F_{\mu 2} = F_{m2} \tag{26}$$

$$F_{\mu 1} = \frac{1}{2}\left[-\frac{G}{h_g}\sqrt{a^2 - \frac{4h_g L}{G}F_{m2}} + \left(\frac{Ga}{h_g} - 2F_{m2}\right)\right] \tag{27}$$

Thus

$$z_3 = \frac{F_{\mu 1} + F_{\mu 2}}{G} = \frac{\left[-\frac{G}{h_g}\sqrt{a^2 - \frac{4h_g L}{G}F_{m2}} + \left(\frac{Ga}{h_g} - 2F_{m2}\right)\right] + 2F_{m2}}{2G} \tag{28}$$

where a is the distance from the center of mass to the front axle.

(4) When the braking severity is greater than z_3, the front and rear axle braking force continues to be distributed according to the ideal braking force distribution curve.

$$F_{\mu 1} = F_{I1}, \quad F_{\mu 2} = F_{I2} \tag{29}$$

Electro-hydraulic braking force allocation

In order to take full advantage of the motor braking force, electro-hydraulic braking force allocation is in accordance with the principle of granting priority to use the motor braking force. When the motor braking force cannot meet the requirements of braking severity, the remaining braking force is supplemented by the hydraulic braking force. The control chart of electro-hydraulic braking force allocation is shown in Figure 16.

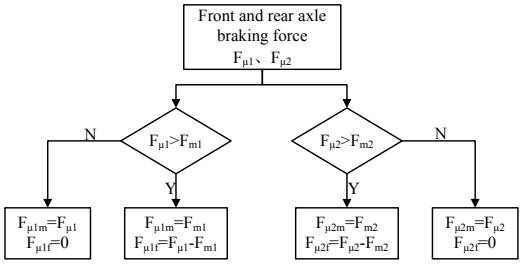

Figure 16. Chart of electro-hydraulic braking force allocation.

The braking force allocation strategy proposed in this paper makes use of the motor braking force as much as possible, especially when the front axle motor braking force cannot meet the braking force demand while there remains a surplus in the rear motor axle braking force. This allocation strategy can reduce the mechanical friction energy loss during the braking process and improve the efficiency of energy recovery.

B. Braking Control Strategy under Emergency Braking

In the case of emergency braking, in order to ensure the safety of the vehicle, the braking force required for the vehicle is all provided by the hydraulic brake force, which means $F_{\mu 1m} = F_{\mu 2m} = 0$ during the emergency braking. A large number of studies have shown that the longitudinal forces and lateral forces between the tire and the ground are affected by the slip rate and there is an optimum slip rate corresponding to a certain road surface (assuming $\lambda_{opt} = 0.2$). At the optimum slip rate, the longitudinal and lateral forces between the tire and the ground are both maintained at a large value.

When the slip rate of the vehicle is greater than 0.1, it is determined that the vehicle enters an emergency braking state. At this time, the fuzzy controller is adopted to control the slip rate of the vehicle in emergency braking. The number of fuzzy controller input variables is called the fuzzy controller's dimension. The higher the dimension of the fuzzy controller, the better the control effect. But the high dimension will also make the control rules complicated and the control algorithm will be difficult to achieve. In this paper, the two-dimensional fuzzy controller is used to control the slip rate of the vehicle. The input of the fuzzy controller is the error E between the actual slip rate and the optimum slip rate, and the change rate EC of the error E. The output is the change amount of the wheel cylinder pressure U. The structure of the fuzzy logic controller is shown in Figure 17.

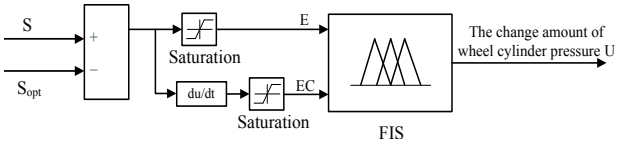

Figure 17. Structure of the fuzzy logic controller.

The membership functions of E, EC and U are shown in Figure 18.

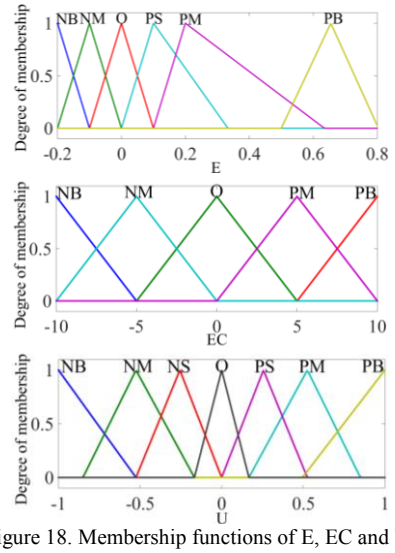

Figure 18. Membership functions of E, EC and U.

The fuzzy rules designed in this paper are shown in TABLE IV.

TABLE IV. FUZZY RULES

U		EC				
		NB	*NM*	*O*	*PM*	*PB*
E	*NB*	PB	PB	PB	PM	PM
	NM	PM	PM	PS	NS	NS
	O	PS	PS	O	NS	NS
	PS	PS	NS	NS	NM	NM
	PM	NS	NS	NM	NB	NB
	PB	NM	NM	NB	NB	NB

IV. SIMULATION AND ANALYSIS

The braking force allocation strategy is validated in the co-simulation platform of Carsim, AMEsim and MATLAB / Simulink. In Carsim, a vehicle model is established and the main parameters of vehicle are shown in TABLE V. Since this paper studies electric vehicles with four IWMs, it is necessary to modify the vehicle driveline in Carsim to an external differential to interrupt the power transmission between the driveline and the wheel, so that the motor braking torque is applied directly to the wheel (Lu et al., 2014). AMESim software contains a wealth of hydraulic components library and has obvious advantages in modeling system including hydraulic components. The model of EHB system is built based on the AMESim platform in this paper (Jin et al., 2011). The control block diagram of the system is shown in Figure 19.

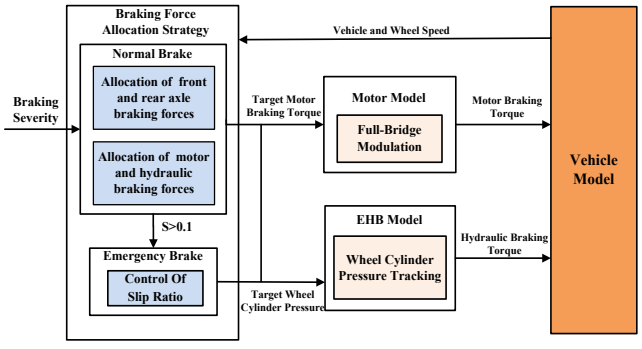

Figure 19. Control block diagram of the system.

TABLE V. VEHICLE PARAMETER

Parameters(units)	Value
m(kg)	1,331
G(N)	13,043.8
L(mm)	2,400
a(mm)	1,040
b(mm)	1,360
h_g(mm)	540
r(mm)	300
T_{rated}(Nm)	85
ω_{rated}(r/min)	1,000
SOC_0（%）	60
Q_r(Ah)	60

A. *Simulation under normal braking*

In order to verify the proposed braking force allocation strategy and observe the dynamic characteristics of the motor under normal braking, the simulation conditions are set as follows: the initial velocity is 60 km/h, the road adhesion coefficient is 0.7, the braking severity is 0.1 and 0.3, respectively. The simulation results are shown in Figure 20 and Figure 21.

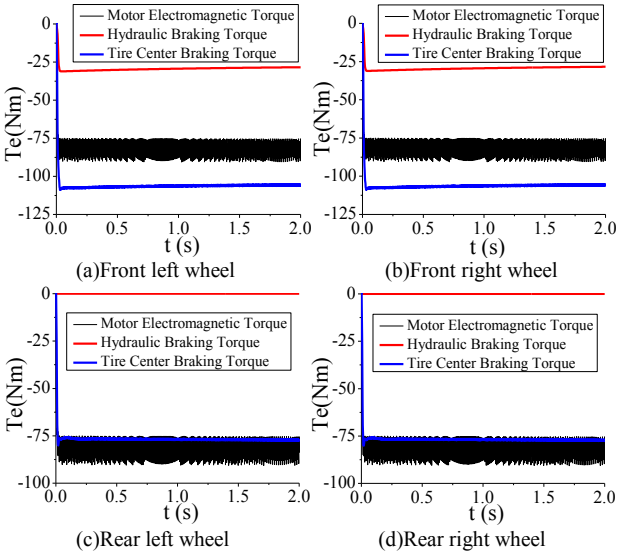

(a)Front left wheel (b)Front right wheel

(c)Rear left wheel (d)Rear right wheel

Figure 20. Braking force allocation results under the braking severity of 0.1.

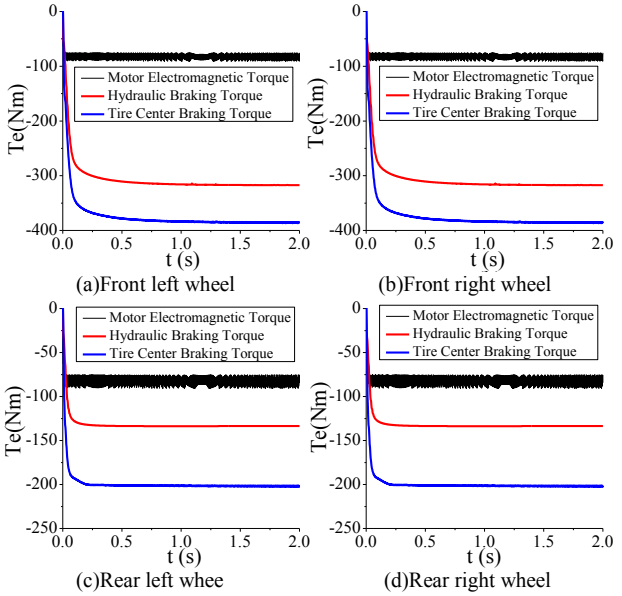

(a)Front left wheel (b)Front right wheel

(c)Rear left whee (d)Rear right wheel

Figure 21. Braking force allocation results under the braking severity of 0.3.

Results analysis: When the braking severity is 0.1, the motor electromagnetic torque and hydraulic braking torque of the front wheel are 85 Nm and 29 Nm respectively, and the motor electromagnetic torque and hydraulic braking torque of the rear wheel are 85 Nm and 0 Nm respectively. It can be seen that the braking force allocation strategy proposed in this paper can allocate the braking force of the front and rear axles according to the maximum braking torque of the motor (Under full-bridge modulation, the maximum motor braking torque is

85Nm). When it comes to the allocation of the electro-hydraulic braking force of each axis, the motor braking force is preferentially adopted to take full use of the motor braking force.

When the braking severity is 0.3, the motor electromagnetic torque and hydraulic braking torque of the front wheel are 85 Nm and 317 Nm respectively, and the electromagnetic torque and hydraulic braking torque of the rear wheel are 85 Nm and 133 Nm respectively. It can be seen that under the medium braking severity, the motor braking force of each axis cannot meet the braking severity requirement and the distributed compound braking system carries on the electro-hydraulic compound brake so that the residual braking force is supplemented by the hydraulic braking force. At the same time, it can be seen from the data of the tire center braking torque that although the motor electromagnetic torque has a torque ripple of about 15 Nm through the full-bridge modulation, the total braking torque measured at the center of the tire is stabilized after filtered by the tire inertia.

B. *Simulation under emergency braking*

In order to ensure the safety of the vehicle, the braking force allocation strategy must be able to control the wheel slip rate in the case of emergency braking. The simulation conditions are as follows: the initial velocity is 60 km/h, the road adhesion coefficient is 0.7, and it assumes that the optimum slip rate is 0.2. The speed/wheel speed curve and the wheel slip rate are shown in Figure 22.

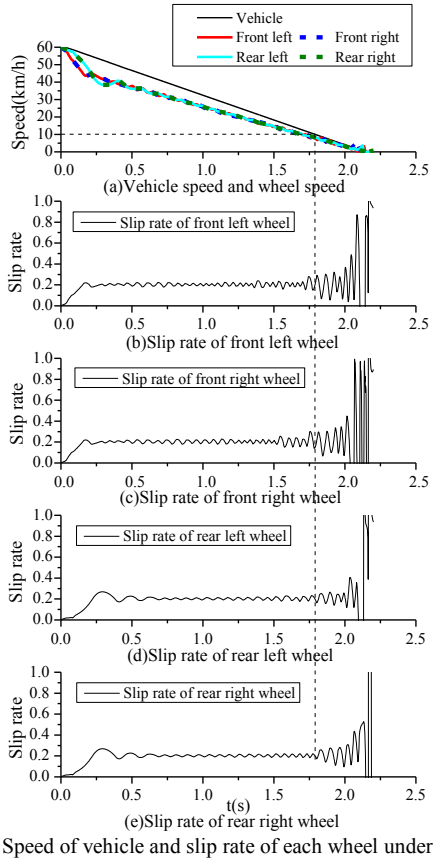

Figure 22. Speed of vehicle and slip rate of each wheel under emergency braking.

Results analysis: At the beginning of the braking process, the system is still in the normal braking state. When the slip rate of the front wheel s > 0.1 and vehicle speed ≥ 10km/h, the system enters the emergency braking state. The slip rate of the vehicle can be maintained at the optimum slip rate by the control of the fuzzy controller.

When the braking time reaches 1.79 s, and vehicle speed < 10km/h, the vehicle has already been slowed down. At this moment, because the vehicle speed is low and wheel speed fluctuates greatly, slip rate has a greater fluctuation.

Simulation results show that the fuzzy controller proposed in this paper can effectively control the slip rate of the wheel in emergency braking to ensure that the vehicle has a large longitudinal and lateral force.

V. CONCLUSION

This paper first analyzes the two common regenerative braking control methods of IWM: half-bridge modulation and full-bridge modulation, and compares the effects of the two methods. Based on the principle of maximum motor braking force, this paper proposes a braking force allocation strategy and establishes the co-simulation platform based on Carsim, MATLAB/Simulink, and AMEsim. The braking force allocation strategy is validated under normal braking and emergency braking conditions. The simulation results show that the braking force allocation strategy proposed in this paper can preferentially adopt the motor braking force and realize the compound braking under the normal braking condition. Under the emergency braking condition, the slip rate can be maintained at the optimum slip rate to ensure the safety of the vehicle. Meanwhile, the dynamic performance of motors is well reflected in the simulation process.

REFERENCES

[1] Gao, Y., L. Chen, and M. Ehsani. "Investigation of the effectiveness of regenerative braking for EV and HEV." Hydroelectric Energy (1999).

[2] Gao, Yimin, and M. Ehsani. "Electronic Braking System of EV And HEV---Integration of Regenerative Braking, Automatic Braking Force Control and ABS." Future Transportation Technology Conference & Exposition 2001.

[3] Wang, Bin, et al. A robust wheel slip control design for in-wheel-motor-driven electric vehicles with hydraulic and regenerative braking systems. 2014.

[4] Xu, Wei, et al. "A regenerative braking control strategy for electric vehicle with four in-wheel motors." Control Conference IEEE, 2016:8671-8676.

[5] LIAN Yu-feng, TIAN Yan-tao, HU Lei-lei, et al. A new braking force distribution strategy for electric vehicle based on regenerative braking strength continuity. Journal of Central South University, 2013, 20(12):3481-3489.

[6] Yu, Jiangze, J. Chen, and Y. Peng. "Observer-based regenerative braking control for Four-Wheel-Independent-Actuated Electric Vehicles." Control Conference IEEE, 2016:8951-8955.

[7] Pillay, P, and R. Krishnan. "Modeling of permanent magnet motor drives." Industrial Electronics IEEE Transactions on 35.4(1987):537-541.

[8] Salameh, Z. M, M. A. Casacca, and W. A. Lynch. "A mathematical model for lead-acid batteries." IEEE Transactions on Energy Conversion 7.1(1992):93-98.

[9] Zhang, Junzhi, et al. "Cooperative control of regenerative braking and hydraulic braking of an electrified passenger car." Proceedings of the Institution of Mechanical Engineers Part D Journal of Automobile Engineering 226.10(2012):1289-1302.

[10] Wu, Dongmei, et al. "Structure Analysis and Pressure Control of Electro-Hydraulic Braking System." 2013 2nd international conference on opto-electronics engineering and materials eesearch 2013:1288-1292.

[11] Lu, Xiong, et al. "Modeling of Distributed Drive Electric Vehicle Based on Co-simulation of Carsim/Simulink."

[12] Jin, Zhi Lin, et al. "Modeling and Analysis of Electro Hydraulic Brake System Based on AMESim/Matlab." Advanced Materials Research 383-390(2011):1994-1999.